Journal of Membrane Science 657 (2022) 120706

Contents lists available at ScienceDirect

Journal of Membrane Science

journal homepage: www.elsevier.com/locate/memsci

Tailoring the substrate of thin film reverse osmosis membrane through a novel β-FeOOH nanorods templating strategy: An insight into the effects on interfacial polymerization of polyamide

Nur Diyana Suzaimi [a], Pei Sean Goh [a,*], Kar Chun Wong [a], Nik Ahmad Nizam Nik Malek [b], Ahmad Fauzi Ismail [a], Jun Wei Lim [c]

[a] Advanced Membrane Technology Research Centre, School of Chemical and Energy Engineering, Universiti Teknologi Malaysia, 81310 Johor, Malaysia
[b] Department of Biosciences, Faculty of Science, Universiti Teknologi Malaysia, 81310 Johor, Malaysia
[c] Department of Fundamental and Applied Sciences, HICoE-Centre for Biofuel and Biochemical Research, Institute of Self-Sustainable Building, Universiti Teknologi PETRONAS, 32610, Seri Iskandar, Perak, Malaysia

ARTICLE INFO

Keywords:
Ferric oxyhydroxides
Porous substrate
Polyamide membrane
Reverse osmosis
Template assisted technique

ABSTRACT

The tailoring of the physico-chemical properties of thin film composite (TFC) membranes is essential to augment their separation performances. Maintaining a good balance between water productivity and rejection is one of the important criteria for efficient water treatment. This work reports a nanomaterial-enabled templating strategy used for the construction of a TFC substrate layer. Beta ferric oxy-hydroxides (β-FeOOH) nanorods were used as a pore forming template for polysulfone (PSf) substrate. The templating strategy using β-FeOOH nanorods increased the porosity and pore space connectivity of the PSf substrate, hence facilitating the formation of homogenous and defect-free polyamide selective layers through interfacial polymerization (IP) on top of the PSf substrate. The best membrane, a-TFC β2 which was fabricated using etched PSf substrate preloaded with 1 wt% β-FeOOH exhibited an increase in water permeance by 3-fold compared to the neat TFC membrane while maintaining NaCl rejection of 97.5%. Furthermore, the templating strategy endowed the membrane with better 72 h operational stability, where the water permeance and selectivity were not much deteriorated compared to that of neat membrane. This study demonstrates the feasibility of using substrate templating technique to finetune the porosity and surface pore properties for an optimized IP reaction and hence, enhancing the desalination performance.

1. Introduction

Water desalination is an essential part of our toolkit in tackling the increasing demand for fresh water. Advancement in pressure-driven membrane separation processes i.e. reverse osmosis (RO) and nanofiltration (NF) provide a beneficial impact on the water shortage crises on account of their potential in offering sustainable and adequate water supply [1–3]. In view of the status quo of current commercial RO desalination, a burgeoning research interest has been dedicated to the design and optimization of membranes and also energy recovery systems to promote RO as a truly sustainable and cost-effective desalination technology. A fundamental understanding of membrane structure–performance relationships is important to design high-performance desalination membranes.

High water permeance should be achieved without the expense of selectivity. However, maintaining high permselectivity remains a challenge in RO operation [4,5]. The typically used RO thin film composite membrane (TFC) membrane consists of a polyamide (PA) thin film selective layer with an underneath porous and mechanically strong substrate layer. The former determines the separation performance of the membrane while the latter acts as a support. The unique structure of TFC minimizes the membrane resistance to water permeation upon filtration. Fine-tuning the properties of the PA layer is a well-attended research topic in this realm. The optimization of PA layer has been touted as a key implementation to maximize membrane water-salt permselectivity [6–8]. Despite the continuous efforts and progresses made in optimizing

* Corresponding author.
E-mail addresses: diyanasuzaimi@yahoo.com (N.D. Suzaimi), peisean@petroleum.utm.my (P.S. Goh), karchun@utm.my (K.C. Wong), niknizam@fbb.utm.my (N.A.N.N. Malek), afauzi@utm.my (A.F. Ismail), junwei.lim@utp.edu.my (J.W. Lim).

https://doi.org/10.1016/j.memsci.2022.120706
Received 10 March 2022; Received in revised form 20 May 2022; Accepted 3 June 2022
Available online 5 June 2022

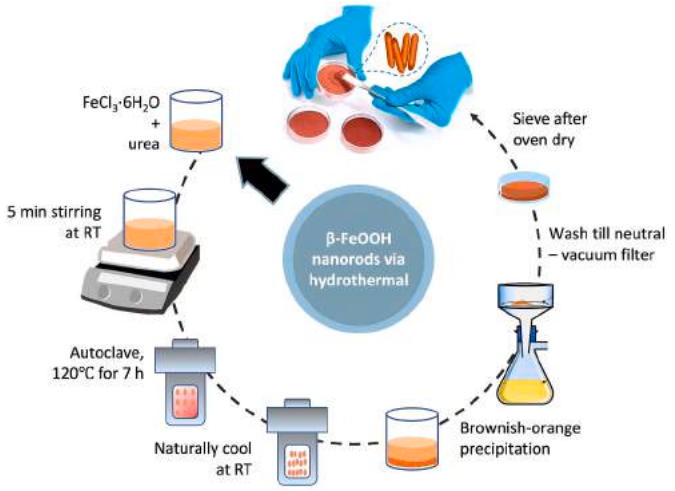

Fig. 1. Synthesis route of β-FeOOH nanorods.

TFC membrane, studies on the substrate layer are also essential as the findings can provide insights into the properties of substrate as a factor affecting the formation of PA layer. While it has been commonly considered that substrate is merely a support that provides mechanical support for the deposition of the ultrathin PA layer, it has been evidenced that the physio-chemical properties of the substrate i.e., pore characteristics, porosity, roughness, and hydrophilicity are of significant importance in developing an ideal TFC membrane [9].

Recent years have witnessed the interest in investigating the effects of the changes in substrate properties and chemistry on the structural and separation performance of PA TFC membranes [5,10,11]. Peng et al. evidenced that the desalination performance of PA TFC membrane is governed by the surface porosity and pore size of substate [10]. Substrate with smaller pore sizes is favorable in preventing PA intrusion into its polymeric matrix thus facilitating the formation of a thin selective layer with a higher water permeance [10,12]. However, despite the efforts made, no consensus has been reached among the studies. Contradictory result and interpretation have been reported where the substrate with large pore size was witnessed to exhibit higher permselectivity and good mechanical durability despite its extremely porous structure [13]. It has also been observed that a highly permeable TFC membrane could only be fabricated with substrate that was dominated with the large pores and high hydrophobicity [14]. Although literatures revealed that morphological and porosity of the substrate surface control the thickness and nodular structure of selective layer to some extent, more comprehensive studies are still desired to accurately disclose the effect of substrate properties on the selective layers so that the properties of the entire membrane can be tailored in more meaningful ways.

In term of TFC substrate modification, most of the efforts reported so far are mainly focused on the embedding nanomaterials as nanofillers to alter the substrate properties [2,15–17]. With the growing concerns on the potential leaching of nanomaterials during the membrane operation, other membrane structure tailoring strategies are desired. Template-assisted method has been proposed to manipulate membrane separation performance using nanomaterials as a template, allowing pore formation and channels upon their removal by simple acid etching and cleaning [18]. The templating of ultrafiltration PSf membrane using $CaCO_3$ nanoparticles improved pore connectivity which in turn resulted in a highly porous membrane [19]. The water permeance was improved about 80%, with the highest value of 353 $Lm^{-2}h^{-1}$ bar^{-1}, compared to the neat membrane. Likewise, MOFs templating agent was found to optimize the microstructure of polyacrylonitrile (PAN) substrate for ultrafiltration. Significantly enhanced water permeance was achieved due to the increase in transfer coefficient of membrane, while the membrane selectivity remain unchanged [20].

The feasibility of using layered double hydroxides (LDHs) as templating agent has been proposed as a concentration polarization control strategy for TFC FO membranes [21]. A highly porous with well interconnected-pore substrate was generated, thereby boosted the FO performance. Yan et al. incorporated silica nanoparticles into TFC RO membrane [22]. The filtration experiments indicated that the templating strategy improved substrate surface porosity and so the pure water flux and salt rejection. However, substrate templating for TFC RO membrane has scarcely been reported as the existing studies largely focused on generating nanovoids inside the PA layer or disrupting the PA network to tune the structural properties [4,5,22]. Compared to spherical zero-dimensional nanoparticles, one-dimensional nanorods possess porous structures that highly interconnected to facilitate water flow channel [23]. Additionally, nanorods can be synthesized via various routes with tailorable morphological and structural properties applications [24,25]. This study adopted β-FeOOH nanorods as a novel templating agent for TFC RO membrane substrate modification. On account of the unique features of one-dimensional β-FeOOH templating agent, the porosity and pore space connectivity of the substrate could be improved to facilitate the formation PA selective layer, which in turn contributes to the improvement in water permeance and salt rejection.

2. Experimental

2.1. Materials

Ferric (III) chloride hexahydrate ($FeCl_3 \cdot 6H_2O$) and urea from Sigma-Aldrich were used for the synthesis of β-FeOOH nanorods. Udels P-3500 PSf pellets (Solvay), polyvinylpyrrolidone (PVP, K30) pore former and 1-methyl-2-pyrrolidinone (NMP, 99.5%) solvent used for membrane substrate fabrication were purchased from Acros Organic. M-Phenylenediamine (MPD, 99%) and 1,3,5-benzenetricarbonyl trichloride (TMC, 98%) from Acros Organic and n-hexane (C_6H_6, 49%) from Merck were used for performing the interfacial polymerization (IP). Sodium chloride (NaCl, 99.5%, Sigma-Aldrich) was used to prepare salt solutions. RO water utilized in membrane performance tests was obtained from Milli-Q ultrapure water system (Millipore, Billerica, MA).

2.2. Synthesis of β-FeOOH nanorods

β-FeOOH nanorods was hydrothermally synthesized [24]. About 2.7 g of ferric chloride ($FeCl_3 \cdot 6H_2O$) and 1.2 g urea was dissolved in 160 mL of DI water. The mixture was constantly stirred to form a homogenous orange solution. Then, the solution was placed into Teflon-lined stainless-steel autoclave, covered, and tighten. The autoclave was then heated up to 120 °C at a rate of 1.5 °C min^{-1} for 7 h. After cooled down, the obtained brownish-orange precipitation was thoroughly washed with RO water to eliminate the residual Cl^- followed by vacuum filtration to obtain the product. Finally, the product was dried overnight in a vacuum drying oven at 40 °C. The schematic diagram of the synthetic route of β-FeOOH nanorods is shown in Fig. 1.

2.3. Fabrication of porous support layer

The dope solution with formulation of PSf: PVP: NMP in the ratio of 17:1:82 wt% was prepared under vigorous stirring for 8 h at room temperature. A homogenous and bubble-free dope solution was obtained after 12 h of constant stirring and deaeration. Using a glass rod, the dope was uniformly cast on a flat glass plate. To complete phase inversion process, the plate was immediately immersed in a water bath for several minutes. The membrane obtained was then soaked in DI water overnight to ensure residual solvent was removed.

Templated substrates were prepared by adding different amounts of β-FeOOH to NMP solvent and subjected to ultrasonication for 30 min to reduce agglomeration. PSf pellets and PVP were added to the mixture

Table 1
Denotation and composition of as-fabricated membranes.

No.	Substrate Layer	TFC membrane	PSf (wt.%)	PVP (wt.%)	NMP (wt.%)	FeOOH (wt.%)	Immersion in HCl
1	PSf	TFC	17	1	82.0	–	–
2	a-PSf	a-TFC	17	1	82.0	–	48 h
3	PSf β1	TFC β1	17	1	81.75	0.50	–
4	a-PSf β1	a-TFC β1	17	1	81.75	0.50	48 h
5	PSf β2	TFCβ2	17	1	81.0	1.00	–
6	a-PSf β2	a-TFC β2	17	1	80.0	1.00	48 h
7	PSf β3	TFCβ3	17	1	81.5	2.00	–
8	a-PSf β3	a-TFC β3	17	1	81.5	2.00	48 h

and the substrate was fabricated through phase inversion technique as described above. The composite substrates were subsequently etched by 1 M HCl solution for 48 h to remove β-FeOOH and form porous spaces within the substrate matrix. Prior to PA layer formation, the substrates were rinsed with DI water to remove the remaining HCl solution.

2.4. Deposition of polyamide selective layer

Reaction of IP was conducted to form a thin PA layer on the PSf substrate. The MPD-impregnated substrate was first prepared by soaking PSf membranes in 2% aqueous MPD solution for 5 min. To complete the IP reaction, excess MPD solution was drained off until no water was observed. 0.1 wt% TMC/hexane solution was coated within 1 min to allow condensation reaction and formation of thin film. Afterwards, the resultant membrane was oven-cured at 60 °C for 3 min and thoroughly rinsed with DI-water. Eventually, the fresh membranes were stored in DI water before testing. Table 1 summarizes the composition and denotation of the membranes fabricated in this study.

2.5. Characterizations

The characterizations of both nanomaterials and membranes were performed to investigate the changes in their physico-chemical properties i.e., surface elemental composition and chemical structure, surface, and cross-section morphologies, as well as surface wettability and surface charge. Phase crystallinity of the as-synthesized β-FeOOH nanorods was analyzed using X-ray radiation diffraction (XRD, Rigaku) using Cu Kα radiation operated at 40 kV and 30 mA, respectively. The nanorods powder was loaded onto the sample holder and the diffraction pattern was scanned at 2θ angle range from 4° to 80°. To capture the detailed morphology of the nanorods, a high voltage 200 kV transmission electron microscope (TEM, HT 770, Hitachi, Japan) was employed. The functional groups of β-FeOOH nanorods were determined by Fourier transform infrared (FTIR) spectroscope with attenuated total reflectance (ATR, Thermo Nicolet Avatar 360). Meanwhile, field emission scanning electric microscope (FESEM, Hitachi SU8020) was used for the determination of morphology and topography of membrane. The membrane samples were coated with platinum prior to the scanning. Energy-dispersive X-ray (EDX) spectroscope was used to analyze the elemental composition of the as-fabricated membrane before and after modification. Also, their chemical compositions were further assessed using X-ray photoelectron spectroscope (XPS, AXIS Supra) with a monochromatic Al-Kα radiation ($h\nu = 1486.6$ eV). Casa XPS software was used to analyze the data. The atomic ratio (r) of oxygen over nitrogen (O/N) obtained was then used to compute their crosslinking degree (CD) based on Eq. (1) [5]:

$$\mathrm{CD} = \frac{4-2r}{1+r}\ x\ 100\% \tag{1}$$

The surface roughness and wettability of membranes were examined using atomic force microscope (AFM, SII Nano Technology SPA 300 HV) and contact angle goniometer (OCA 15 Pro, Dataphysics), respectively. The contact angle measurements were taken 1 s after the droplet in contact with the membrane surface.

Based on the SEM images, further analysis was carried out using Image-J software to determine the surface porosity and pore structure of PSf substrate [26]. Notably, throughout the analysis the contrast and threshold levels of all images were kept constant. Three replicate images were analyzed, and the average value was reported. The surface porosity ε (%) was calculated from Eq. (2).

$$\varepsilon = \frac{S_p}{S_m} \times\ 100\% \tag{2}$$

where S_p (nm^2) is the total area of pores and S_m (nm^2) is the area of substrate surface in the same surface image.

The total porosity (ε_t) of the substrate was determined gravimetrically by weighing the membrane sample with known area and thickness. The average of 3 replicates was obtained by using Eq. (3).

$$\varepsilon_t = \frac{((W_w - W_d)\ |\ \rho_{water})}{V} \tag{3}$$

where w_w is the total weight of membrane after wetting with DI water while w_d is the weight of dry membrane, ρ_{water} is the density of water, and V is the total volume of membranes.

2.6. TFC membrane performance testing

Membrane performance encompasses water permeance and salt rejection were tested using a lab-scale dead-end stirred filtration system (Sterlitech Corp (Kent, WA). The membrane sample with 0.00146 m^2 effective area (A_m) was compacted by filtration of RO water at 16 bar feed pressure for 30 min. After stabilization for another 30 min at 15 bar (δP), the water permeated rate (Q in L h^{-1}) through the cell was measured and the water permeance of the selective layers was quantified by the water permeance coefficient (A, L m^{-2} h^{-1} bar^{-1}) as calculated from Eq. (4):

$$\textit{Water permeance},\ A\ \left(\mathrm{L\ \ m^{-2}\ \ h^{-1}\ \ bar^{-1}}\right) = \frac{Q}{A_m \Delta P} \tag{4}$$

Using the same membrane, the selectivity was determined by filtering 2000 ppm NaCl solution. Accordingly, the feed solution conductivity (C_f) and permeate solution (C_p) was measured using conductivity meter (Model 4520, Jenway). The calculation of NaCl rejection was made based on Eq. () as the conductivity was linearly correlated to the NaCl concentration. In addition, based on solution-diffusion theory, salt permeability, B (L m^{-2} h^{-1}) was calculated using Eq. (5). Δπ indicates the osmotic pressure difference between the permeate and the feed solutions while (δP in bar) is transmembrane pressure. The average value was reported based on the triplicates of each membrane.

$$\textit{Salt rejection},\ R\ (\%) = \left(1 - \frac{C_p}{C_f}\right) \times\ 100\% \tag{5}$$

$$\textit{Salt permeability},\ B\ \left(L\ m^{-2}\ h^{-1}\right) = A\frac{1-R}{R}\ (\Delta P - \Delta\pi) \tag{6}$$

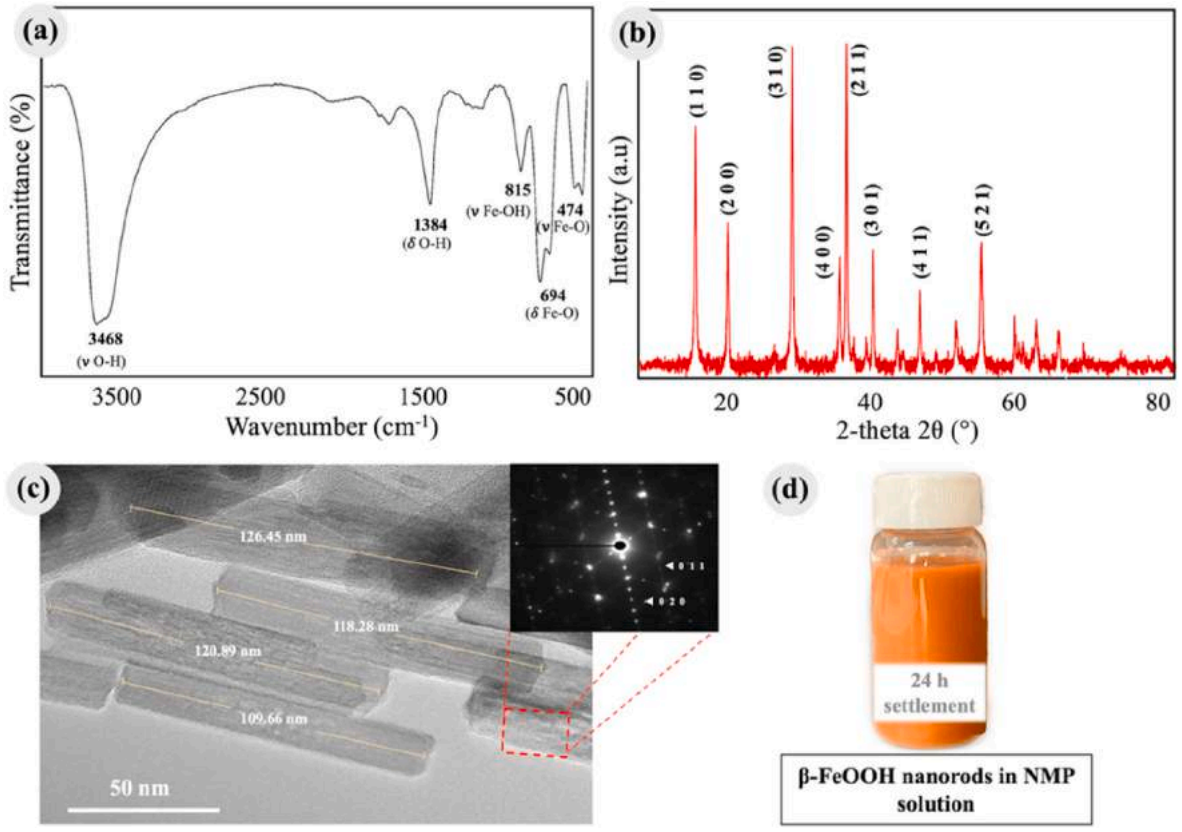

Fig. 2. (a) FTIR spectra, (b) XRD pattern, (c) TEM images captured at × 300 k (inset is the corresponding electron diffraction (SAED) patterns) of the as-synthesized β-FeOOH nanorods and (d) the dispersibility of β-FeOOH in NMP solvent.

Another essential characteristic for practical application is the stability of membrane under long term filtration. A prolonged 72 h cross-flow filtration was conducted to assess the stability of the modified membranes prepared in this study. The filtration system equipped with permeation cell (CF042P, Sterlitech Corp., USA) of 0.00442 m^2 effective area, water pump and flow meter was used. After compaction and stabilization, the water permeance of membrane was recorded every 30 min at 15 bar for up to 72 h. Thereafter, the feed was replaced with 10 L of 2000 mg L^{-1} NaCl aqueous solution and the membrane NaCl rejection was recorded every 30 min. Both water permeance as well as NaCl rejection recorded at every 30 min was dividing with respective initial value to obtained normalized values.

3. Results and discussion

3.1. Characterization of β-FeOOH nanorods

FTIR spectrum shown in Fig. 2a provides information about functional groups presents in the nanorods. The adsorption peak at 3468 cm^{-1} is associated to the OH stretching vibrations of physically absorbed water or structural OH groups present on the surface plane of β-FeOOH nanorods [27]. Meanwhile, the peak at 1384 cm^{-1} is ascribed to the deforming of OH groups. The characteristic Fe–O bending and stretching vibrations of β-FeOOH are indicated by the appearance of peaks at 694 and 474 cm^{-1}, respectively. Additionally, the peak at 815 cm^{-1} can be associated to the Fe–O–OH bending vibrations [27].

The result of XRD pattern is presented in Fig. 2b. The presence of (110), (200), (310), (400), (211), (301), (411), and (521) reflection planes indicated the formation of tetragonal phase of β-FeOOH [24,28]. The sharp and intense diffraction peaks indicated the as synthesized nanorods is well-crystallized. The structural and morphological features of the nanorods were further investigated through TEM. As demonstrated in Fig. 2c, the rod-like β-FeOOH exhibited homogeneous size distribution with length and diameter of approximately 120 nm and 20 nm, respectively [24,28,29]. Previous studies have demonstrated that substrate layer with approximately 20–30 nm pore diameter was favorable to fabricate a TFC membranes with balanced permeance and salt rejection [30,31]. Hence, it can be deduced that the well dispersed β-FeOOH nanorods with that desired diameter can serve as an appropriate templating agent upon membrane fabrication. Inset of Fig. 2c shows the corresponding electron diffraction (SAED) pattern, indicating the crystal facet of (221) planar with d-spacing of 2.53 Å, which is in accordance with the XRD results.

The prepared β-FeOOH nanorods were dispersed in NMP solvent (2 mg mL^{-1}) under ultrasonication for 30 min. From Fig. 2d, β-FeOOH nanorods shows a good dispersion in NMP solution with no sediment observed after 24 h suggesting that suspension exhibited high stability. The good interfacial interaction between β-FeOOH and NMP solvent is desired to facilitate a good dispersion and the preparation of a homogenous PSf dope solution [32,33].

3.2. Characterization of thin film composite membrane

Fig. 3a schematically illustrates the simple fabrication routes of PA TFC membrane using PSf substrate templated with β-FeOOH nanorods. The β-FeOOH acts as a template to construct porous networks within the PSf substrate upon its removal through acid etching. The crosslinked and defect-free PA layer was expected to form on the substrate surface as a result of interface reaction between two immiscible monomers i.e. MPD aqueous and TMC organic phase during the IP [34]. The EDX mapping shown in Fig. 3b confirmed the presence of Fe and O in the substrate layer. Upon HCl etching, the characteristic peaks of Fe diminished, implying that most β-FeOOH nanorods have been thoroughly removed from the substrate of a-TFC β1 and a-TFC β2. Low intensity of Fe peak

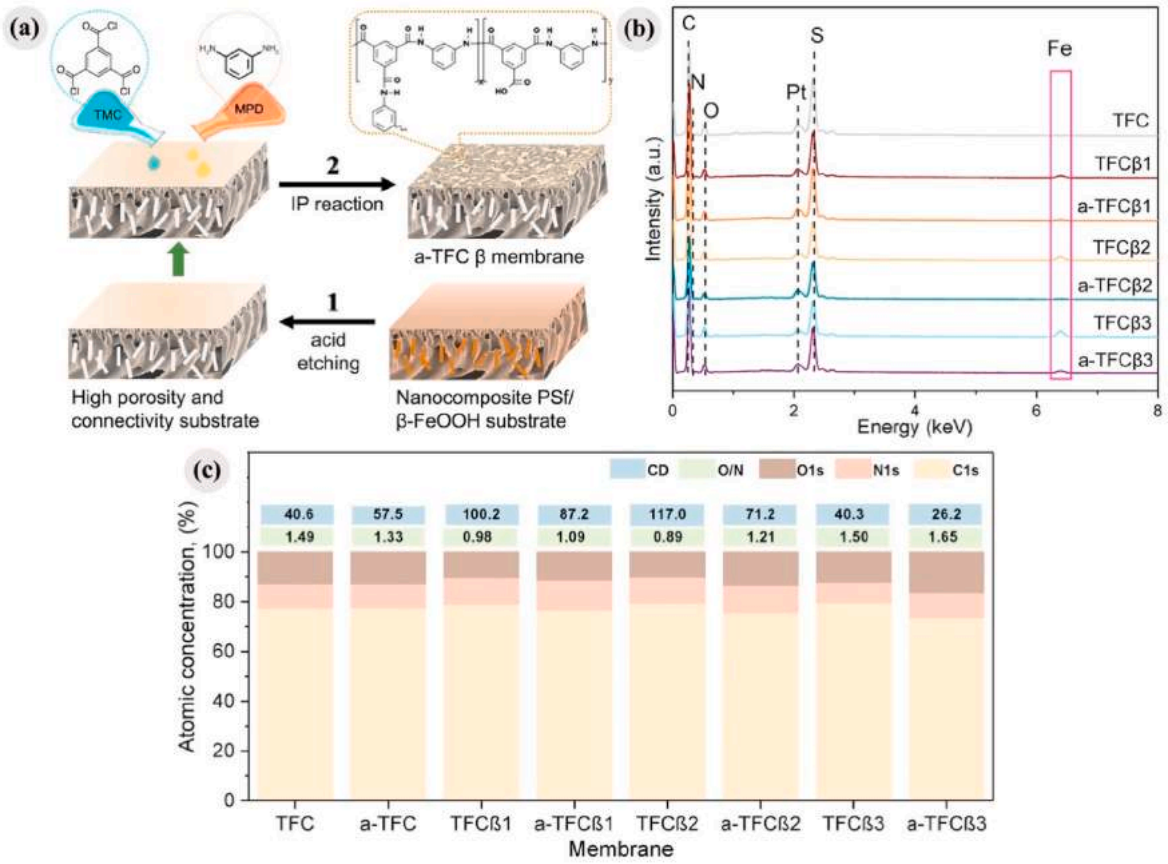

Fig. 3. (a) Schematic illustration of the preparation of a PA TFC membrane with the substrate templated with β-FeOOH nanorods. (b) EDX mapping of membranes; (c) Relative elemental breakdown with atomic ratio of O/N and crosslinking degree as determined by XPS.

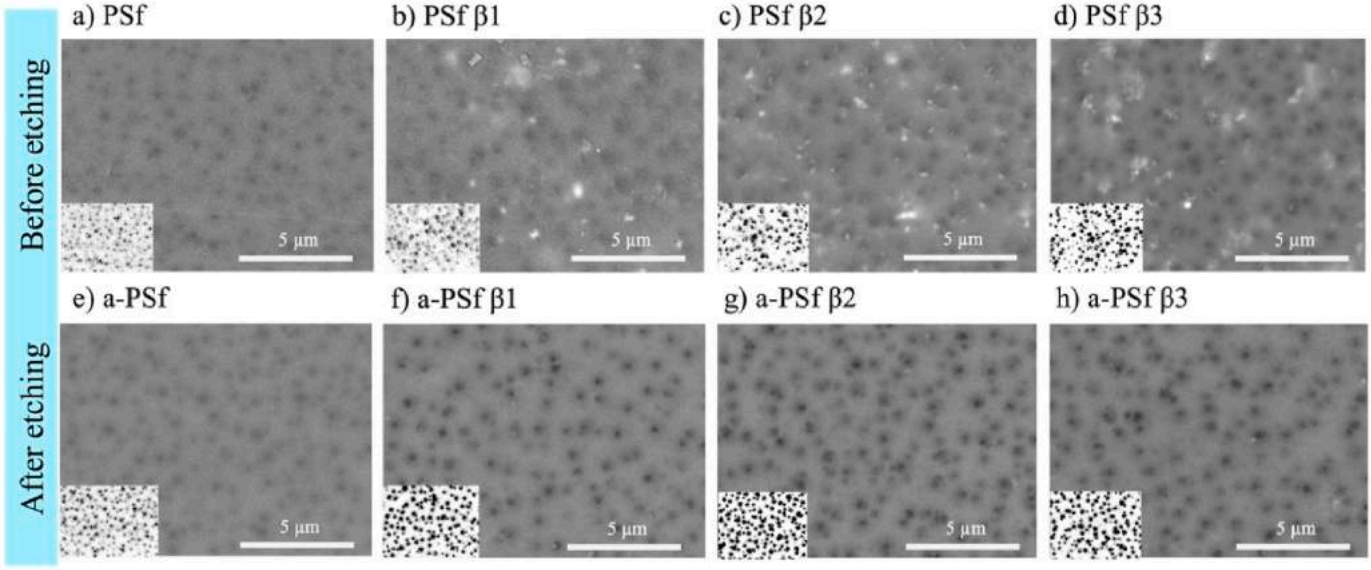

Fig. 4. Top view SEM images of substrate before and after etching. Insets are the adjusted contrast of the micrographs.

was however observed. This might also attribute to the improper rinse of membrane after the etching process, leaving some Fe residues on the surface. The presence of N element, which is the major composition of PA layer, suggested the interfacial crosslinking has been established between the aqueous and organic monomers [35].

To further determine the chemical state and atomic composition i.e., C1s, N1s and O1s of the PA layer, high-resolution XPS surface analysis was performed. Since the penetration depth for XPS is of less than 10 nm, no Fe element was detected from the spectra. Fig. 3c presents the XPS results in terms of elemental breakdown with ratio of O/N and CD of the PA layer. Lower O/N corresponds to more cross-linked PA [5]. The CD increased with the incorporation of β-FeOOH, from 40.6% of the neat

Table 2
Surface textural analysis of substrates templated with β-FeOOH.

Substrate	Pore density (pores/μm^2)	Surface porosity (%)	Total porosity (%)
PSf	11.5	13.6	57.2
a-PSf	13.0	15.2	65.6
PSf β1	15.5	15.0	65.8
a-PSf β1	19.0	25.2	81.3
PSf β2	23.3	17.7	66.4
a-PSf β2	24.5	26.5	84.1
PSf β3	8.9	14.9	68.8
a-PSf β3	32.2	23.3	89.2

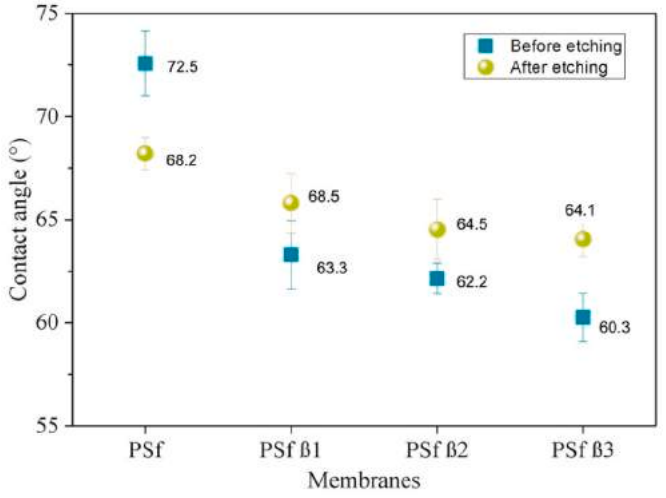

Fig. 5. Water contact angle of β-FeOOH incorporated substrates before and after acid etching.

TFC to 100% of TFC β1 and 117.0% of TFC β2, suggested the formation of well-crosslinked PA layer atop of membranes. After acid etching, a-TFC β1 and a-TFC β2 showed a lower O/N ratio with CD increased by more than 50% in relative to neat TFC membranes. The formation of denser PA layer was due to the enhanced and uniform amine diffusion, which facilitated a strong interaction between substrate and PA layer [2]. Denser PA layer could better hinder the transport of the salt across RO membrane, thereby rendering high salt retention.

3.2.1. *Surface properties of substrate layer*

The surface morphologies of the neat and nanocomposite substrate are shown in Fig. 4 In contrast to the surface of neat substrate (PSf), the nanocomposite substrate before etching (PSf β1, PSf β2 and PSf β3) showed the presence of β-FeOOH on the substrate surface. These particles were almost completely removed upon the acid etching. The rod-like structure cannot be clearly seen from the top surface due to the embedment of β-FeOOH within the polymer matrix. However, better magnification image of PSf β3 substrate in Fig. S1, verified the random distribution of nanorods in the polymer matrix. Data from image analysis was also used to plot surface pore size distribution (PSD) (Fig. S2). The mean pore size of membranes after β-FeOOH addition increased from 0.26 μm to 0.33 μm. After nanorod templating, the a-TFC membranes exhibited well-defined pores with regular shape.

The pore density and surface porosity of the substrates are tabulated in Table 2. For the β-FeOOH-embedded substrates, the surface porosity and pore density increased with the increasing β-FeOOH content but decreased for PSf β3 with the loading of 2.0 wt %. On the other hand, the total porosity increased steadily with the increasing β-FeOOH content. The observation suggested that β-FeOOH played a role as hydrophilic additives in which its presence has accelerated the rate exchange between solvent and non-solvent during phase inversion, thus favouring the formation of porous structure with voids. However, the excessive loading of β-FeOOH (PSf β3) increased the casting solution viscosity which in turn slowed down the exchange rate and subsequently reduced the surface porosity and pore density porosity [36].

The porosity and pore density of the substrates were significantly improved upon acid etching. This suggested that the removal of the templating agent from the substrate has created the templated micropores. Whilst their surface porosity and total porosity followed the trend similar to that of unetched substrates, the pore density steadily increased from 13 pores/μm^2 for a-PSf to 32.2/μm^2 for a-PSf β3. The trend suggested that templating strategy using β-FeOOH left many voids behind substrate pores, hence effectively improved pore within the substrate. In particular, pore density showed an improvement as high as ~60% by a-PSf β3 compared to that of a-PSf. The surface porosity of a-PSf β2 is 26.5%, followed by a slight reduction for a-PSf β3 (23.3%) but higher than that of neat. In this combination, the desired pore density can

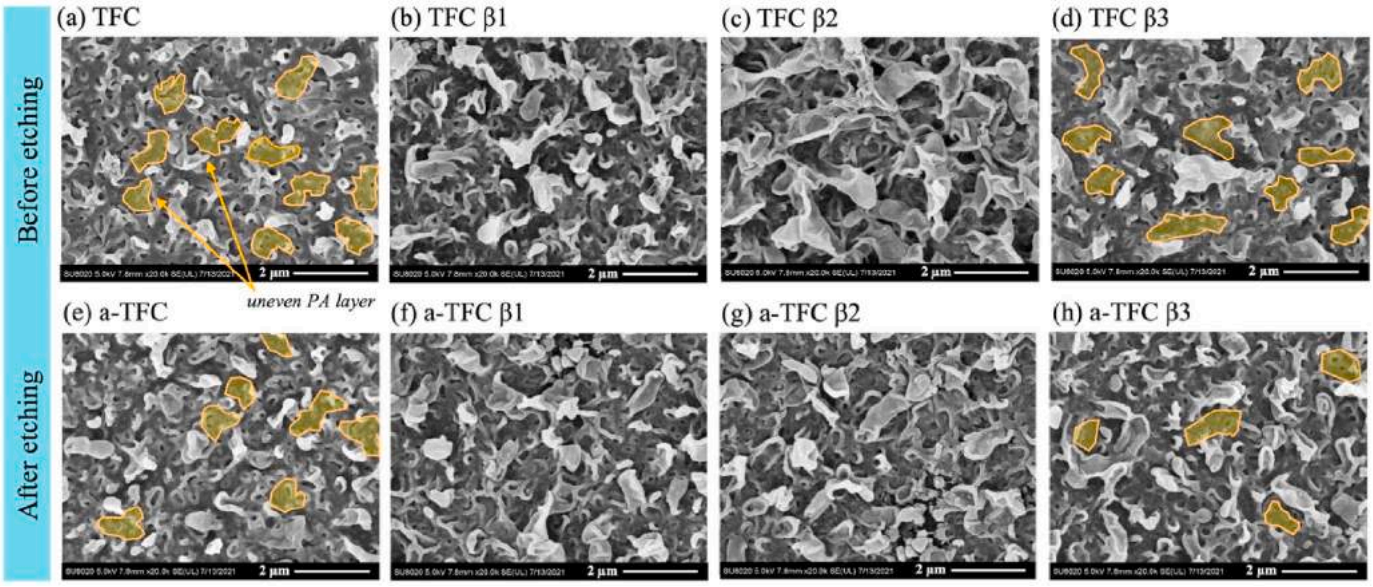

Fig. 6. FESEM (× 20 k) of various polyamide formed on the TFC membranes.

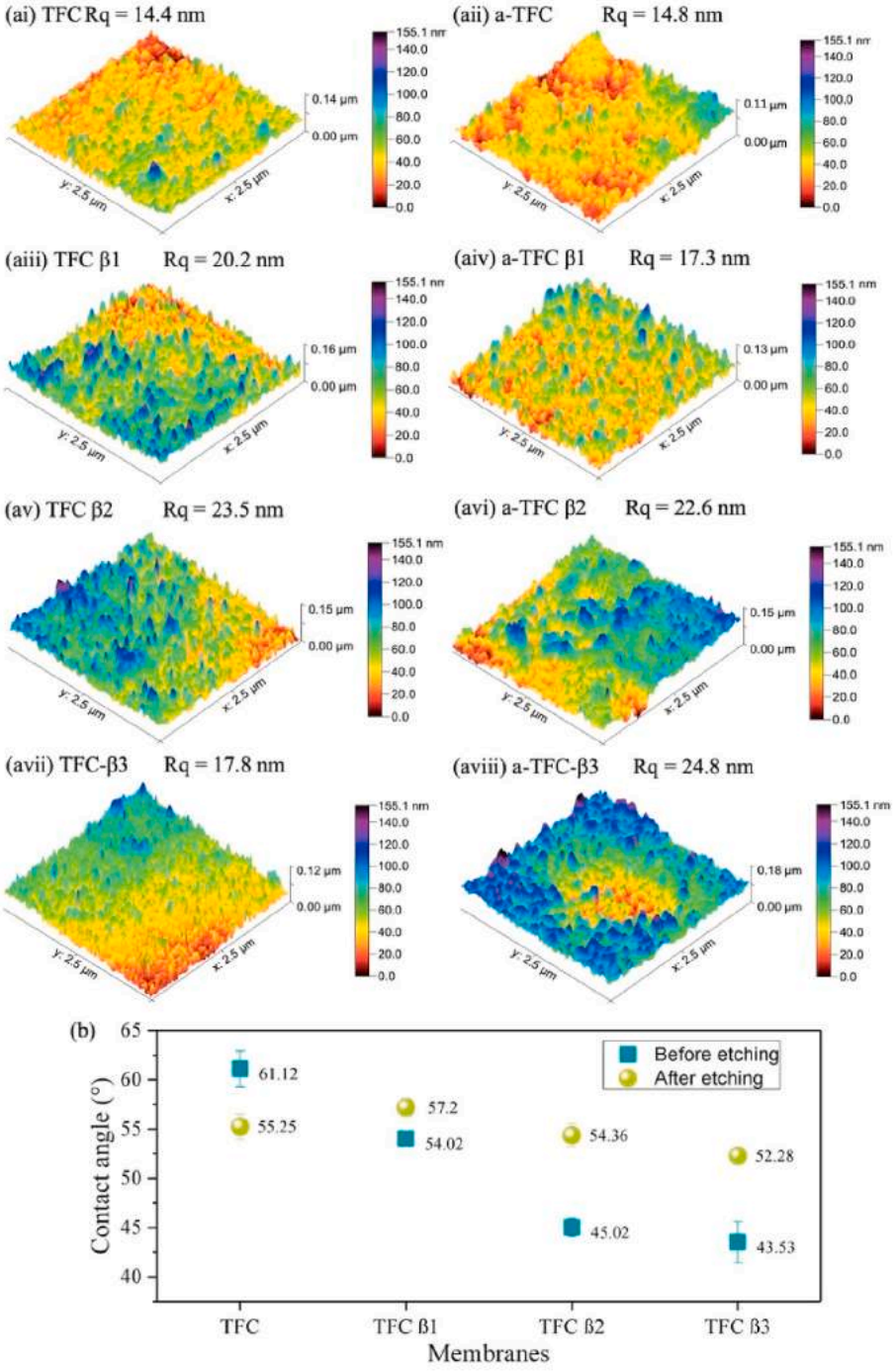

Fig. 7. (a) AFM micrographs of the PA layer prepared over different substrates; (b) Water contact angles of the resultant TFC membranes.

preserve high surface porosity that is beneficial for promoting IP reaction [10]. Furthermore, such modification develops a highly porous structure where the total porosity enhanced significantly as observed on a-PSf β1 (57.2–81.3%), a-PSf β2 (57.2–84.1%), and a-PSf β3 (57.2–89.2%). By considering the textural properties, a-PSf β2 with 1 wt % β-FeOOH templating agent could be considered as the best substrate as the substrate characterized by high surface porosity and pore number density is beneficial to promote water passage and rejection during membrane filtration [36]. During the interfacial polymerization of monomers to form PA layer, the desired porous structure promotes significant diffusivity of amine monomers toward the reaction zone. Besides, the newly formed surface pores interconnected with those in the sublayer is beneficial to create new channels that can allow water molecules to slide through membrane. Interestingly, compared to other pore templating agents e.g., silica [30,36], LDHs [21], and zinc oxides [23] with the same loading, one-dimensional β-FeOOH in nanorods structure demonstrated better textural properties, i.e. higher substrate porosity and pore space connectivity. It could be inferred that the geometry of nanostructured templating agent plays a role in altering microstructure of the substrate layer.

Contact angle is influenced by both surface chemical composition e.g., hydrophobic/hydrophilic functional groups as well as surface topology and roughness [21]. Referring to Fig. 5, the average water contact angle of neat TFC and a-TFC substrates were 72.6° and 68.2°, respectively. In line with literatures, with the incorporation of β-FeOOH templating agent, the contact angle value decreased to 65.3°, 62.2° and

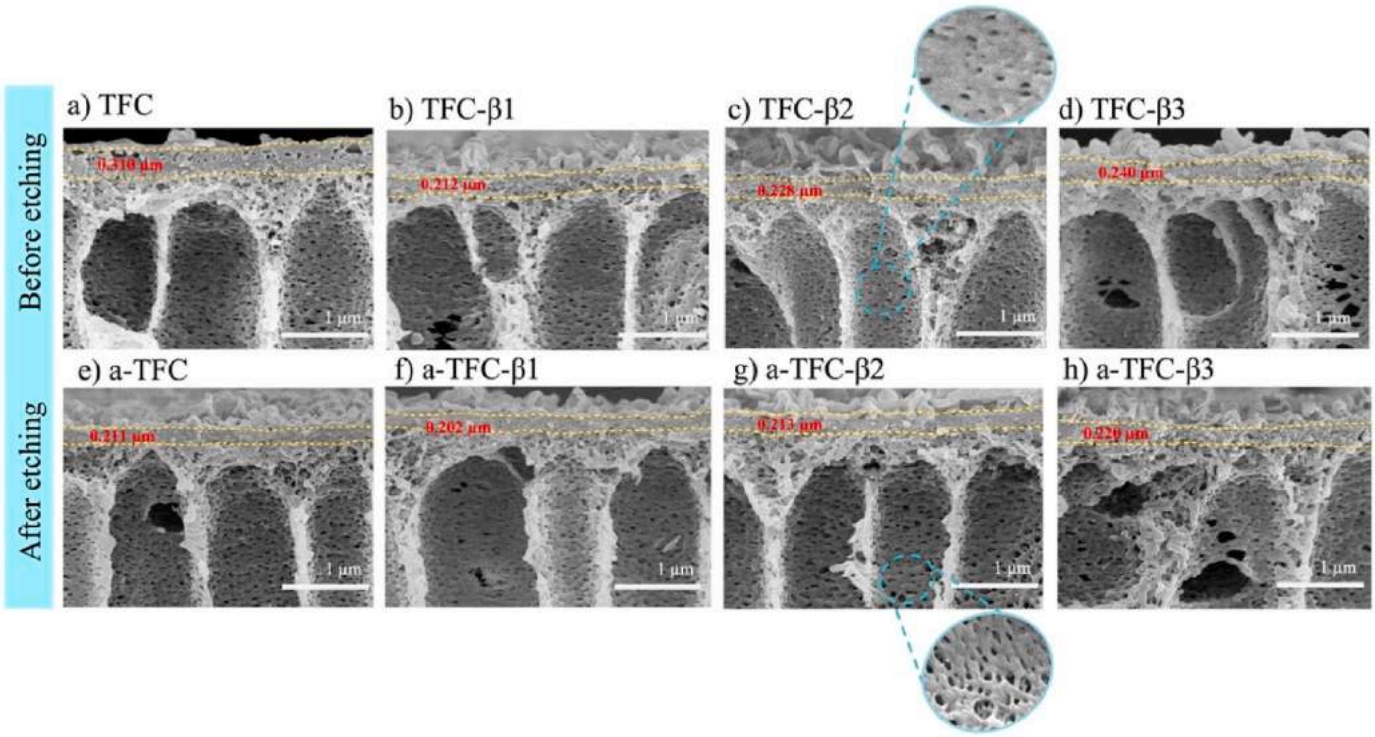

Fig. 8. Cross sectional features illustrating morphologies of the substrate (inset is enlarged interconnected pores) and the average thickness PA selective layer before and after etching.

60.3° for TFC β1, TFC β3 and TFC β3, respectively, suggesting that β-FeOOH has rendered greater wettability (hydrophilic) to the membrane on account of the oxygen-rich functional groups [7,37]. Hydrophilic β-FeOOH reduced the interfacial energy between membrane surface and water, hence creating a better water-membrane interaction [38,39]. Given that the surface hydrophilicity of the acid etched substrate showed little discernible differences with the neat substrate, it can be deduced that most of the β-FeOOH have been successfully removed.

3.2.2. *Structural and surface properties of TFC membrane*

The modification of TFC substrate layer should be accomplished without significantly sacrifices the selectivity of the PA layer. To investigate the impact of β-FeOOH templating on the formation of the PA, surface morphology of the TFC membranes were captured and shown in Fig. 6. The surface morphology of all the TFC membranes exhibited a similar structure that typically characterized as ridge-and-valley structure. It appeared as typical dense nodules at the base and leaf-like structure extending to the upper part of the selective layer [2,40]. Such features were originated from the interfacial degassing of CO_2 that are encapsulated between the PA layer and the substrate layer [5,6]. Nevertheless, the hydrophilicity and porosity of the PSf substrate has considerably increased the migration speed of MPD monomer to react with TMC during IP [41]. More heat was generated during the IP reaction and disrupted the interfacial stability, thereby creating a broadened leaf-like structure as observed in TFC β1 and TFC β2 [10]. On the contrary, the PA layer of neat TFC and TFC β3 exhibited smoother surface with less visible ridge-and valley structures, as observed in the highlighted yellow region of Fig. 6 (a, d, e, and h). During the IP, surface with lower pore density adsorbed less MPD which led to the uneven distribution of MPD [12]. Consequently, the PA formed was characterized by lower crosslinking degree and smoother texture.

Upon acid etching, the leaf-like structures of PA become smaller due to retarded IP reaction rate. The substrate with high pore density resulted in the adherence of higher amount of amine onto the substrate surface hence inhibiting the diffusion rate of MPD to react with TMC. As a result, the leaf-like structure of PA shrunk compared to that of TFC. Due to the improved amine distribution, an even PA layer was formed on the substrate. An uneven and defective PA layer was observed for a-TFC β3as the PA layer was formed over large substrate pores that have resulted in loss of the confinement effect [10,42,43]. Large substrate surface pores allowed more PA formed within the pores, hence reducing the membrane permeance [10].

The effects of β-FeOOH-templating on the topology and surface roughness of the PA layer of TFC membranes were further investigated. The morphological and roughness characteristics of TFC and a-TFC modified membranes are shown in Fig. 7a. The root mean square roughness (R_q) was calculated from the height profile of each membrane image. The R_q roughness of TFC (14.4 nm), TFC β1 (20.2 nm) and TFC β2 (23.5 nm). The upward trend suggests the increasing loading of β-FeOOH led to high surface roughness. The observation is also in good agreement with Cassie-Baxter model where the increased surface roughness also led to more wettable surface of the TFC membranes (Fig. 7b) [42,44]. With the presence of PA layer, all TFC membranes showed lower water contact angle values, ranging from ~61° to ~43°. The introduction of –COOH, –NH, and –CONH– via IP was responsible for the enhanced membrane hydrophilicity [7]. The surface roughness of TFC β3 decreased to 17.8 nm probably due to uneven, defective PA layer, and hence smooth membrane surface observed [43]. In addition, it was observed that after acid etching, the R_q values slightly decreased but an increasing trend was still observed with the increasing loading of β-FeOOH. This suggests that a continuous PA layer has covered the entire substrate surface. The increase in R_q can be associated to the increase of effective area available for water transport which may contribute to enhanced water permeation [10,30].

Fig. 8 presents the cross-sectional micrographs of the TFC membranes. It is observed that the PA layer of TFC membrane (Fig. 8a) features a relative flat surface (thickness about 0.3 μm) which suggests that the PA layer penetrated the substrate pores. For TFC β1, the formed PA layer exhibited a distinct ridge-and-valley structure with greater height compared to others and beneficial to maximizing membrane

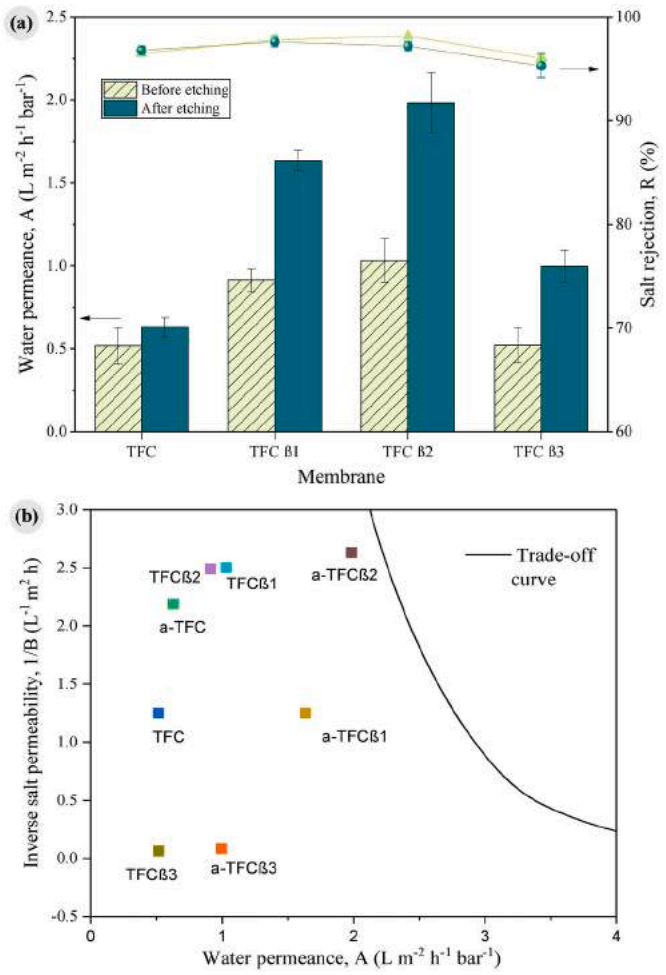

Fig. 9. (a) Water permeance and NaCl rejection of various TFC and a-TFC membranes (operated at 1.5 MPa); (b) Plot of inverse solute permeability (1/B) versus water permeance (A) of the prepared TFC membranes.

selectivity [44]. A thicker PA layer, specifically the basal layer (indicated by the dotted line) formed upon the addition of β-FeOOH templating agent was ascribed to the increase of MPD-TMC reaction rate, hence the PA layer tends to grow thicker on the nanocomposite membrane [5,21,31]. With the increment of β-FeOOH loading, the thickness of the PA layer increased steadily from 0.212 μm to 0.228 μm and 0.240 μm for TFC β1, TFC β1 and TFC β1, respectively. Upon the removal of the templating agent, the decrease of the thickness of basal layer from ~0.212 μm for TFC β1 to ~0.202 μm for a-TFC β1 was due to the thinning effect of the polymeric network resulted from the acid etching [30]. Also, after acid etching, it can be postulated that the higher substrate porosity led to thicker PA layer, from 0.211 μm for a-TFC to 0.220 μm for a-TFC β3. This suggests that substrate modification controlled the release of amine monomers to react with organic monomer, where high amine to acid chloride ratio promote crosslinking degree, thereby a thicker and denser selective layer was formed. Among the modified TFC membranes, the most thick and dense PA layer was observed for TFC β3, that might be the primary barrier for water transport and deteriorate the rejection. The variations of the PA morphology strongly implied that the textural and morphological characteristics of the substrate can considerably affect the PA layer formation [21,36].

The cross-sectional FESEM images (Fig. 8b, d, f, and h) also confirmed that the substrate layers are characterized by finger-like pores that can favorably provide preferential flow channels for water passage [2]. Besides increasing the overall porosity, templating technique has generated extra pores and better connectivity between finger-like pore channels (see inset images Fig. 8c and g). The presence of macropores and the creation of new channels in the substrate facilitated IP reaction to create such dense and thin PA layer that is desired for high salt rejection [21,23].

3.3. Desalination performances of TFC membranes

Evaluating the desalination performance of TFC membranes, the water permeance and salt rejection achieved are depicted in Fig. 9. Overall, similar trend was observed for membranes with etched substrate and unetched substrate but the TFC membranes with etched substrate achieved better water permeance in a range of 0.60–2.05 L $m^{-2}h^{-1}$ bar^{-1} and decent NaCl rejections of 94–97%. It is therefore suggested that before the acid etching, the wettability and surface roughness of the substrate layer played a more dominant role on the formation of the highly selective layer that warrant a satisfactory desalination performance. The neat TFC membrane exhibited water permeance of 0.517 L $m^{-2}h^{-1}$ bar^{-1} with NaCl rejection of 96.5%. Low water permeance of neat TFC membrane might be attributed to the thicker PA layer. The a-TFC membrane showed a marginal increment of ~14% in its permeance compared to that of neat TFC membrane in response to the enhanced pore density and porosity of substrate.

By comparison, TFC membranes fabricated from unetched substrates demonstrated higher permeance and rejection than that of neat TFC membrane but decreased in the order of TFC β1 > TFC β2 ≫ TFC β3. About two-fold increase in water permeance was observed for both TFC β1 and TFC β2 in relative to neat TFC. The improvement can be attributed to the distribution of the hydrophilic β-FeOOH in the PSf matrix which enhanced the membrane wettability and facilitated finger-like

Table 3
The effects of substrate layer (before and after etching) on the PA layer properties and the desalination performance.

Increased hydrophilicity of substrate layer							
Membrane	Substrate hydrophilicity	MPD diffusion	PA thickness (nm)	PA roughness (nm)	PA O:N ratio	Performance A (L $m^{-2}h^{-1}$ bar^{-1})	R (%)
TFC	**61.1°**	**-**	**0.310**	**14.4**	**1.49**	**0.517**	**96.5**
TFC β1	↓	↑	↓	↑	↓	↑ (~61%)	↑ (~1.3%)
TFC β2	↓	↑	↓	↑	↓	↑ (~60%)	↑ (~2.0%)
TFC β3	↓	↓	↓	↓	↑	↕	↕

Increased surface porosity & pore density of substrate layer								
Membrane	Porosity (%)	pore density (pores/μm2)	MPD diffusion	PA thickness (nm)	PA roughness (nm)	PA O:N ratio	Performance A (L $m^{-2}h^{-1}$ bar^{-1})	R (%)
TFC	**57.2**	**11.5**	**-**	**0.310**	**14.4**	**1.49**	**0.517**	**96.5**
a-TFC	↑	↑	↓	↓	↑	↓	↑ (~17%)	↕
a-TFC β1	↑	↑	↓	↓	↑	↓	↑ (~68%)	↑ (~1.1%)
a-TFC β2	↑	↑	↓	↓	↑	↓	↑ (~74%)	↕
a-TFC β3	↑	↑	↓	↑	↑	↓	↓ (~40%)	↓ (~1.3%)

*(↑ is increased, ↓ is decreased and ↕ is maintained in relative to TFC membrane).

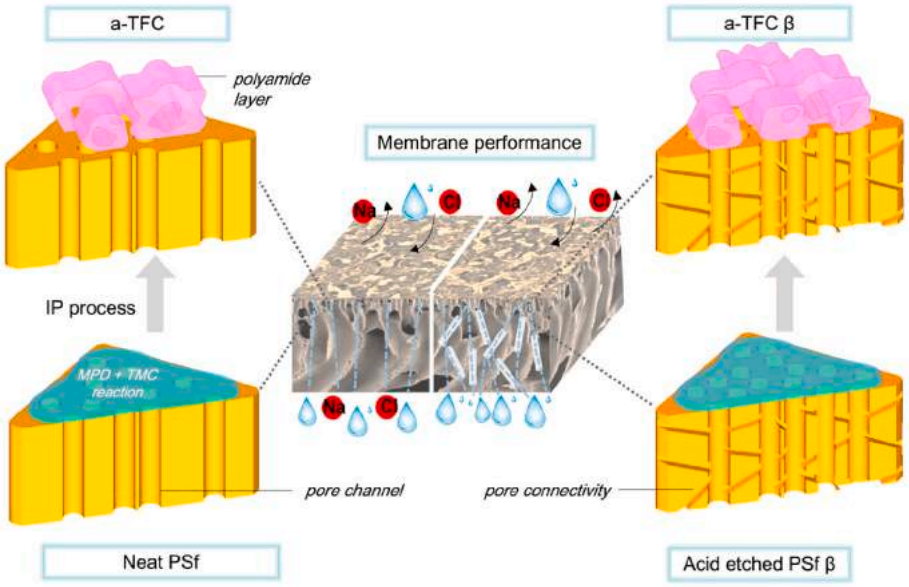

Fig. 10. Schematic illustration of the change in pore channel and pore connectivity upon substrate templating using β-FeOOH.

layers of porous water channels formation [2,45]. Also, the larger ridges and valley presence at the surface would enhance water permeance by increasing the effective contact area between water molecules and the membrane surface [46]. The highest rejection of TFC β2 of 98.5% could be correlated to its highest degree of crosslinking as indicated in Fig. 3c. Deteriorated desalination performance was observed for TFC β3, showing comparable water permeance and NaCl rejection as TFC. This phenomenon was mainly due to the thick PA layer that increased the water diffusion resistance hence obstructing the water permeance [12,21]. Also, high loading of nanoparticles in the substrate of TFC β3 may result in pore blockage hence reducing the permeable area [47]. The relatively low rejection of TFC β3 membrane was mainly due to of the defective PA layer.

As shown in Fig. 9a, water permeance of TFC membranes with etched substrates was improved greatly due to the architecture of the substrate porosity and pore structure [21,23,36]. The water permeance of a-TFC membranes increased in the order of a-TFC < a-TFC β1 < a-TFC β3 and a-TFC β2 attributable to the improved water diffusion across the membrane of higher substrate porosity and pore connectivity. The interconnected pores created new channels to facilitate water transported through the substrate [48]. Among the membranes fabricated in this study, a-TFC β1 and a-TFC β2 outperformed the other membranes with water permeance of 1.63 L m^{-2} h^{-1} bar^{-1} and 2.05 L m^{-2} h^{-1} bar^{-1}, respectively without compromising their rejection (~97.0%). On the other hand, an undesirable loss of water permeance and NaCl rejection was observed for a-TFC β3, which was mainly resulted from the formation of excessive macropores and porosity that impaired the integral PA rejection layer during operation. The PA probably trapped into the substrate pores, imparting additional resistance that hampered water transport [5].

In this study, the performance comparison plot between TFC and a-TFC membranes in terms of water permeance coefficient and inverse salt permeability is presented in Fig. 9b. The plot indicates the trade-off challenge experienced by membranes as they lay below the trade-off line (calculation based on equation of $1/B = 136.35\ A^{-3}$ [44]). From a permselectivity view, a-TFC β2 displays the best performance as it lies relatively closer to the permselectivity tradeoff curve, where enhanced water permeance at a constant and acceptable salt rejection was observed. Mathematically, the membrane has better permselectivity ratio (A/B) as represented by the higher A coefficient paired with higher 1/B, exhibiting minimal trade-off impact. The combination of ideal substrate with the desired textural properties i.e., chemistry and pore properties and optimal PA network of highly crosslinked and rigid layer can synergistically improve the ability to transport water molecules while selectively rejecting ions. Nevertheless, the selectivity of the membranes must be improved further to attain >99% salt rejection without compromising the permeance to ensure the commercial attractiveness of the TFC RO membranes.

The findings from our studies emanated that trade-off between permeance and rejection can be coordinated by fine-tuning the substrate while keeping the same fabrication conditions of the IP procedure. Unlike membrane permeance, which has a strong dependency on substrate porosity and wettability, the dependence of solute rejection on the porosity was more disparate as shown by a-TFC β1, a-TFC β2 and a-TFC β3. Table 3 summarizes the effect of substrate layer on the PA layer properties and the desalination performance normalized to that of neat TFC. By investigating two different substrates (with and without templating agent), it can be concluded the performance achieved by membranes are related to the combination effect of all these aspects. Overall, the features of substrate surface affected the formation of PA layer, specifically the distribution of MPD in the substrate, the MPD diffusivity from substrate to organic phase and consequently the reaction with TMC.

As schematically illustrated in Fig. 10, upon the removal of templating agent through acid etching, an optimized surface pore structures i.e., the high surface porosity and pore number density of substrate have favored the IP reaction and enhanced the PA layer formation. Other factors such as the increase in surface hydrophilicity, surface roughness and the inclusion of additional pathways in the membrane structure due to high porosity and interconnected pores have concertedly contributed to the enhancement in water permeance.

3.4. Assessment of membrane stability

To elucidate the long-term stability of the substrate modified membrane, the best performing membrane in this work was further assessed for its filtration performance for 72 h using a crossflow filtration system. The changes in both water permeance and NaCl rejection as a function of time are presented as normalized water permeance and normalized rejection, respectively, as shown in Fig. 11. Relatively stable performance was observed with time for a-TFC β2 with slight performance decline in their water permeance whilst maintaining the normalized

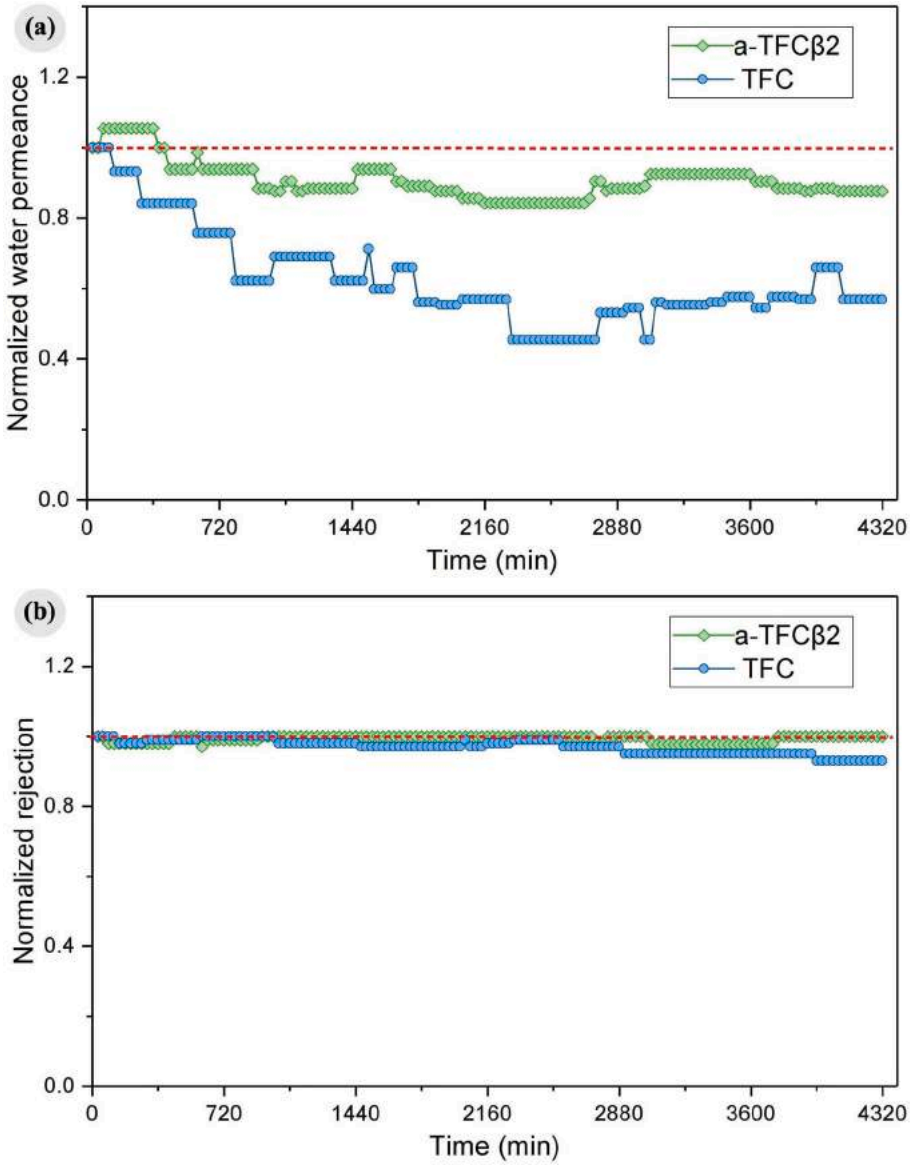

Fig. 11. Changes of membrane performance of a-TFC β2 and TFC over 72 h RO filtration.

value close to 1. The minor changes in normalized water permeance with time were mainly due to membrane compression over long period of filtration. On the other hand, the NaCl rejection ability of a-TFC β2 membrane falls in the range of 98.5%–97% and was maintained throughout the filtration. An unstable performance has been observed for TFC membrane. The normalized permeance was less than 0.5 after 38 h and the NaCl rejection reduced to only 92% at the end of experiment. The significant membrane compaction has induced high resistance for water diffusion. The better long-term performance of a-TFC β2 membrane indicated that the templating technique rendered desired structural properties for both substrate and PA layer without jeopardizing the overall stability of the resultant TFC membrane. Despite the creation of more porous substrate structures and thinner PA layer, the membranes did not suffer from noticeable compaction under 72 h duration and 15 bar operating pressure.

Mechanical stability of the optimized membrane, a-TFC β2 was further analyzed. The tensile strength of the TFC membrane increased from 6.3 MPa for TFC to 8.9 MPa for a-TFC β2. The modification also led to a greater elasticity (elongation at break) 25.2% and 34.5% from a-TFC β2. Although a-TFC β2 membrane has higher porosity compared to neat TFC membrane, it has an adequate mechanical stability i.e., high tensile strength and high elongation at break due to its regularly arranged substrate layer structure (Fig. S3) [13]. The presence of stable macrovoids at the top and bottom of substrate evenly support the pressure exerted and hence, enhance its durability for long term usage thus supporting the stability test performance (Fig. 11) [13]. As depicted in Table 4, in terms of water permeance and long-term performance, a-TFC β2 membrane was superior to TFC membranes reported in other studies. The as-fabricated membrane can serve as an attractive candidate for practical RO process based on its separation performance and high mechanical stability.

4. Conclusion

In summary, key finding of this study deepens the understanding of the influence of templating agent on the structural and textural properties of the substrate of TFC-RO membranes. The hydrophilicity, porosity, and pore density of the β-FeOOH templated PSf substrate altered the diffusion and reaction during the IP process and consequently changed the PA layer features i.e., cross-linking degree, surface roughness, and its thickness. Among the membranes fabricated in this study, a-TFC β2 membrane showed the best combination of productivity

Table 4
Performance comparisons of water permeance, NaCl rejection and separation stability between a-TFC β2 membrane and other modified TFC membranes.

Membrane	Water permeance, (L m^{-2} h^{-1} bar^{-1})	NaCl rejection (%)	Operating condition	Separation stability	Ref.
TFC	0.52	96.5	NaCl: 2000 ppm Pressure: 15 bar	Duration: 72 h Permeance:↓ significantly Rejection: 97-92%	This work
a-TFC β2	2.05	97.0	NaCl: 2000 ppm Pressure: 15 bar	Duration: 72 h Permeance: ↓ slightly Rejection: 97–99%	This work
TFN-SiO_2	0.99	96.8	NaCl: 2000 ppm Pressure: 15 bar	Duration: 24 h Permeance: ↓ slightly Rejection: 96–98%	[49]
TFC-HPμS	1.62	99.0	NaCl: 3500 ppm Pressure: 55 bar	Duration: 24 h Permeance: ↓ slightly Rejection: 96–98%	[13]
LbL-TNS TFC	0.8	98.5	NaCl: 2000 ppm Pressure: 15 bar	Duration: 24 h Permeance: ↓ slightly Rejection: 96-94%	[8]
TFC LDH-HCl	19.3	88.4	NaCl: 2000 ppm Pressure: 5 bar	Not reported	[21]
TFC -PEI	6	97.2	NaCl: 2000 ppm Pressure: 15.5 bar	Not reported	[44]
TFN/TiO_2	1.57	96.5	NaCl: 2000 ppm Pressure: 15 bar	Not reported	[50]

with highest water permeance of 2.05 L $m^{-2}h^{-1}$ bar^{-1} and promising salt rejection of 97%. This was attributable to the increased porosity and pore density of the substrate through β-FeOOH templating that affords a more permeable membrane with good rejection efficiency as the transport pathway of water molecules were shorten through integral PA network. The optimized TFC membrane demonstrated a good long-term stability which is attractive for expanding their application spectrum. This study provides a clear insight in tailoring TFC RO membranes to suppress the water permeance and salt rejection trade-off. By considering the performance, synthesis process of β-FeOOH and the ease of acid etching, the strategy developed in this study is feasible for the fabrication of a scalable and more stable TFC membranes to target different applications.

Authorship contribution statement

All persons who meet authorship criteria are listed as authors, and all authors certify that they have participated sufficiently in the work to take public responsibility for the content, including participation in the concept, design, analysis, writing, or revision of the manuscript. Furthermore, each author certifies that this material or similar material has not been and will not be submitted to or published in any other publication before its appearance in the Journal of Membrane Science (JMS).

Nur Diyana Suzaimi: Investigation, Writing, Data curation. Pei Sean Goh: Supervision, Writing – review & editing, Data curation. Kar Chun Wong: Methodology, Conceptualization. Nik Ahmad Nizam: Writing – review & editing. Jun Wei Lim; Supervision. Ahmad Fauzi Ismail: Funding acquisition.

Declaration of competing interest

The authors declare that they have no known competing financial interests or personal relationships that could have appeared to influence the work reported in this paper.

Acknowledgments

The authors gratefully acknowledge financial support given by the Malaysian Ministry of Higher Education under Malaysia Research University Research Grant 4L862.D:\MYFILES\ELSEVIER\MEMSCI\00120706\S-CEEDITING\gs5

Appendix A. Supplementary data

Supplementary data to this article can be found online at https://doi.org/10.1016/j.memsci.2022.120706.

References

[1] G. Amy, N. Ghaffour, Z. Li, L. Francis, R.V. Linares, T. Missimer, S. Lattemann, Membrane-based seawater desalination: present and future prospects, Desalination 401 (2017) 16–21, https://doi.org/10.1016/j.desal.2016.10.002.
[2] S.C. Mamah, P.S. Goh, A.F. Ismail, N.D. Suzaimi, N.A. Ahmad, W.J. Lee, Flux enhancement in reverse osmosis membranes induced by synergistic effect of incorporated palygorskite/chitin hybrid nanomaterial, J. Environ. Chem. Eng. 9 (2021), 105432, https://doi.org/10.1016/j.jece.2021.105432.
[3] M.Q. Seah, W.J. Lau, P.S. Goh, A.F. Ismail, Greener synthesis of functionalized-GO incorporated TFN NF membrane for potential recovery of saline water from salt/dye mixed solution, Desalination 523 (2022), 115403, https://doi.org/10.1016/j.desal.2021.115403.
[4] Z. Yang, X. Huang, X. Ma, Z. Zhou, H. Guo, Z. Yao, S.-P. Feng, C.Y. Tang, Fabrication of a novel and green thin-film composite membrane containing nanovoids for water purification, J. Membr. Sci. 570 (2019) 314–321, https://doi.org/10.1016/j.memsci.2018.10.057, 571.
[5] W. Li, Z. Yang, W. Liu, Z. Huang, H. Zhang, M. Li, X. Ma, C.Y. Tang, Z. Xu, Polyamide reverse osmosis membranes containing 1D nanochannels for enhanced water purification, J. Membr. Sci. 618 (2021), 118681, https://doi.org/10.1016/j.memsci.2020.118681.
[6] L.E. Peng, Z. Yao, X. Liu, B. Deng, H. Guo, C.Y. Tang, Tailoring polyamide rejection layer with aqueous carbonate chemistry for enhanced membrane separation: mechanistic insights, chemistry-structure-property relationship, and environmental implications, Environ. Sci. Technol. 53 (2019) 9764–9770, https://doi.org/10.1021/acs.est.9b03210.
[7] H.-Z. Zhang, Z.-L. Xu, Q. Shen, High-performance nanofiltration membrane intercalated by FeOOH nanorods for water nanofiltration, Desalination 498 (2021), 114802, https://doi.org/10.1016/j.desal.2020.114802.
[8] N.A. Ahmad, P.S. Goh, K.C. Wong, A.K. Zulhairun, A.F. Ismail, Enhancing desalination performance of thin film composite membrane through layer by layer assembly of oppositely charged titania nanosheet, Desalination 476 (2020), 114167, https://doi.org/10.1016/j.desal.2019.114167.
[9] F. Liu, L. Wang, D. Li, Q. Liu, B. Deng, A review: the effect of the microporous support during interfacial polymerization on the morphology and performances of a thin film composite membrane for liquid purification, RSC Adv. 9 (2019) 35417–35428, https://doi.org/10.1039/c9ra07114h.
[10] L.E. Peng, Z. Yao, Z. Yang, H. Guo, C.Y. Tang, Dissecting the role of substrate on the morphology and separation properties of thin film composite polyamide membranes: seeing is believing, Environ. Sci. Technol. 54 (2020) 6978–6986, https://doi.org/10.1021/acs.est.0c01427.
[11] Z. Wang, Z. Wang, S. Lin, H. Jin, S. Gao, Y. Zhu, J. Jin, Nanoparticle-templated nanofiltration membranes for ultrahigh performance desalination, Nat. Commun. 9 (2018), https://doi.org/10.1038/s41467-018-04467-3.
[12] S.H. Park, S.J. Kwon, M.G. Shin, M.S. Park, J.S. Lee, C.H. Park, H. Park, J.H. Lee, Polyethylene-supported high performance reverse osmosis membranes with enhanced mechanical and chemical durability, Desalination 436 (2018) 28–38, https://doi.org/10.1016/J.DESAL.2018.02.007.
[13] Y.J. Lim, J. Lee, T.-H. Bae, J. Torres, R. Wang, Feasibility and performance of a thin-film composite seawater reverse osmosis membrane fabricated on a highly porous microstructured support, J. Membr. Sci. 611 (2020), 118407, https://doi.org/10.1016/j.memsci.2020.118407.

[14] A.K. Ghosh, E.M. V Hoek, Impacts of support membrane structure and chemistry on polyamide-polysulfone interfacial composite membranes, J. Membr. Sci. 336 (2009) 140–148, https://doi.org/10.1016/j.memsci.2009.03.024.
[15] Y. Wang, B. Gao, S. Li, B. Jin, Q. Yue, Z. Wang, Cerium oxide doped nanocomposite membranes for reverse osmosis desalination, Chemosphere 218 (2019) 974–983, https://doi.org/10.1016/j.chemosphere.2018.11.207.
[16] X. Qian, N. Li, Q. Wang, S. Ji, Chitosan/graphene oxide mixed matrix membrane with enhanced water permeability for high-salinity water desalination by pervaporation, Desalination 438 (2018) 83–96, https://doi.org/10.1016/j.desal.2018.03.031.
[17] H.M. Park, K.Y. Jee, Y.T. Lee, Preparation and characterization of a thin-film composite reverse osmosis membrane using a polysulfone membrane including metal-organic frameworks, J. Membr. Sci. 541 (2017) 510–518, https://doi.org/10.1016/j.memsci.2017.07.034.
[18] N.D. Suzaimi, P.S. Goh, A.F. Ismail, S.C. Mamah, N.A.N.N. Malek, J.W. Lim, K. C. Wong, N. Hilal, Strategies in forward osmosis membrane substrate fabrication and modification: a review, Membranes 10 (2020) 332, https://doi.org/10.3390/membranes10110332.
[19] S. Zhang, J. Zhou, Z. Wang, J. Xia, Y. Wang, Preparation of polysulfone-based block copolymer ultrafiltration membranes by selective swelling and sacrificing nanofillers, Front. Chem. Sci. Eng. (2021), https://doi.org/10.1007/s11705-021-2038-x.
[20] J.-Y. Lee, C.Y. Tang, F. Huo, Fabrication of porous matrix membrane (PMM) using metal-organic framework as green template for water treatment, Sci. Rep. 4 (2014) 3740, https://doi.org/10.1038/srep03740.
[21] P. Lu, W. Li, S. Yang, Y. Wei, Z. Zhang, Y. Li, Layered double hydroxides (LDHs) as novel macropore-templates: the importance of porous structures for forward osmosis desalination, J. Membr. Sci. 585 (2019) 175–183, https://doi.org/10.1016/j.memsci.2019.05.045.
[22] X.-H. Ma, Z.-K. Yao, Z. Yang, H. Guo, Z.-L. Xu, C.Y. Tang, M. Elimelech, Nanofoaming of polyamide desalination membranes to tune permeability and selectivity, Environ. Sci. Technol. Lett. 5 (2018) 123–130, https://doi.org/10.1021/acs.estlett.8b00016.
[23] X. Zhao, J. Li, C. Liu, Improving the separation performance of the forward osmosis membrane based on the etched microstructure of the supporting layer, Desalination 408 (2017) 102–109, https://doi.org/10.1016/j.desal.2017.01.021.
[24] X.L. Fang, Y. Li, C. Chen, Q. Kuang, X.Z. Gao, Z.X. Xie, S.Y. Xie, R. Bin Huang, L. S. Zheng, pH-induced simultaneous synthesis and self-assembly of 3D layered β-FeOOH nanorods, Langmuir 26 (2010) 2745–2750, https://doi.org/10.1021/la902765p.
[25] M.O. Akharame, B.O. Fagbayigbo, O. Pereao, O.U. Oputu, D.I. Olorunfemi, O. S. Fatoki, B.O. Opeolu, Beta-FeOOH nanoparticles: a promising nano-based material for water treatment and remediation, J. Nanoparticle Res. 23 (2021) 8, https://doi.org/10.1007/s11051-020-05117-w.
[26] L. Huang, J.R. McCutcheon, Impact of support layer pore size on performance of thin film composite membranes for forward osmosis, J. Membr. Sci. 483 (2015) 25–33, https://doi.org/10.1016/j.memsci.2015.01.025.
[27] M. Karami-Darehnaranji, S.M. Taghizadeh, E. Mirzaei, A. Berenjian, A. Ebrahiminezhad, Size tuned synthesis of FeOOH nanorods toward self-assembled nanoarchitectonics, Langmuir 37 (2021) 115–123, https://doi.org/10.1021/acs.langmuir.0c02466.
[28] A. Samanta, S. Das, S. Jana, Exploring β-FeOOH nanorods as an efficient adsorbent for arsenic and organic dyes, ChemistrySelect 3 (2018) 2467–2473, https://doi.org/10.1002/slct.201703022.
[29] H. Wu, C. Wang, J. Kwon, Y. Choi, J. Lee, Synthesis of 2D and 3D hierarchical β-FeOOH nanoparticles consisted of ultrathin nanowires for efficient hexavalent chromium removal, Appl. Surf. Sci. 543 (2021), 148823, https://doi.org/10.1016/j.apsusc.2020.148823.
[30] J. Li, Q. Liu, X. Li, Y. Liu, J. Xie, Template-assisted fabrication of thin-film composite forward-osmosis membrane with controllable internal concentration polarization, Ind. Eng. Chem. Res. 55 (2016) 5327–5334, https://doi.org/10.1021/acs.iecr.6b00874.
[31] M. Rastgar, A. Bozorg, A. Shakeri, Novel dimensionally controlled nanopore forming template in forward osmosis membranes, Environ. Sci. Technol. 52 (2018) 2704–2716, https://doi.org/10.1021/acs.est.7b05583.
[32] S.C. Mamah, P.S. Goh, A.F. Ismail, M.A.M. Amin, N.A. Ahmad, N.D. Suzaimi, Y. O. Raji, Facile preparation of palygorskite/chitin nanofibers hybrids nanomaterial with remarkable adsorption capacity, Mater. Sci. Eng. B. 262 (2020), 114725, https://doi.org/10.1016/j.mseb.2020.114725.
[33] P. Lu, S. Liang, L. Qiu, Y. Gao, Q. Wang, Thin film nanocomposite forward osmosis membranes based on layered double hydroxide nanoparticles blended substrates, J. Membr. Sci. 504 (2016) 196–205, https://doi.org/10.1016/j.memsci.2015.12.066.
[34] M. Mohammadifakhr, J. de Grooth, H.D.W. Roesink, A.J.B. Kemperman, Forward osmosis: a critical review, Processes 8 (2020) 404, https://doi.org/10.3390/PR8040404.
[35] K.H. Lasisi, K. Zhang, Polyamine-based thin-film composite nanofiltration membrane embedded with catalytic chemical additive for enhanced separation performance and acid stability, J. Membr. Sci. 644 (2022), 120155, https://doi.org/10.1016/J.MEMSCI.2021.120155.
[36] W. Yan, Z. Wang, J. Wu, S. Zhao, J. Wang, S. Wang, Enhancing the flux of brackish water TFC RO membrane by improving support surface porosity via a secondary pore-forming method, J. Membr. Sci. 498 (2016) 227–241, https://doi.org/10.1016/j.memsci.2015.10.029.
[37] L. Zhang, Y. He, L. Ma, J. Chen, Y. Fan, S. Zhang, H. Shi, Z. Li, P. Luo, Hierarchically stabilized PAN/β-FeOOH sanofibrous membrane for efficient water purification with excellent antifouling performance and robust solvent resistance, ACS Appl. Mater. Interfaces 11 (2019) 34487–34496, https://doi.org/10.1021/acsami.9b12855.
[38] Kumar Mahdi, Perdicakis Goswami, Sadrzadeh Shankar, Robust polymer nanocomposite membranes incorporating discrete TiO2 nanotubes for water treatment, Nanomaterials 9 (2019) 1186, https://doi.org/10.3390/nano9091186.
[39] H. Zarrabi, M.E. Yekavalangi, V. Vatanpour, A. Shockravi, M. Safarpour, Improvement in desalination performance of thin film nanocomposite nanofiltration membrane using amine-functionalized multiwalled carbon nanotube, Desalination 394 (2016) 83–90, https://doi.org/10.1016/j.desal.2016.05.002.
[40] W. Kuang, Z. Liu, H. Yu, G. Kang, X. Jie, Y. Jin, Y. Cao, Investigation of internal concentration polarization reduction in forward osmosis membrane using nano-CaCO3 particles as sacrificial component, J. Membr. Sci. 497 (2016) 485–493, https://doi.org/10.1016/j.memsci.2015.06.052.
[41] L. Wang, M. Kahrizi, P. Lu, Y. Wei, H. Yang, Y. Yu, L. Wang, Y. Li, S. Zhao, Enhancing water permeability and antifouling performance of thin–film composite membrane by tailoring the support layer, Desalination 516 (2021), 115193, https://doi.org/10.1016/J.DESAL.2021.115193.
[42] X. Li, Q. Li, W. Fang, R. Wang, W.B. Krantz, Effects of the support on the characteristics and permselectivity of thin film composite membranes, J. Membr. Sci. 580 (2019) 12–23, https://doi.org/10.1016/j.memsci.2019.03.003.
[43] L. Shen, X. Zhang, L. Tian, Z. Li, C. Ding, M. Yi, C. Han, X. Yu, Y. Wang, Constructing substrate of low structural parameter by salt induction for high-performance TFC-FO membranes, J. Membr. Sci. 600 (2020), 117866, https://doi.org/10.1016/j.memsci.2020.117866.
[44] Y.J. Lim, K. Goh, G.S. Lai, Y. Zhao, J. Torres, R. Wang, Unraveling the role of support membrane chemistry and pore properties on the formation of thin-film composite polyamide membranes, J. Membr. Sci. 640 (2021), 119805, https://doi.org/10.1016/j.memsci.2021.119805.
[45] N. Ma, J. Wei, R. Liao, C.Y. Tang, Zeolite-polyamide thin film nanocomposite membranes: towards enhanced performance for forward osmosis, J. Membr. Sci. 405 (2012) 149–157, https://doi.org/10.1016/j.memsci.2012.03.002, 406.
[46] B. Khorshidi, T. Thundat, B.A. Fleck, M. Sadrzadeh, A novel approach toward fabrication of high performance thin film composite polyamide membranes, Sci. Rep. 6 (2016) 1–10, https://doi.org/10.1038/srep22069.
[47] Y. Wen, J. Yuan, X. Ma, S. Wang, Y. Liu, Polymeric nanocomposite membranes for water treatment: a review, Environ. Chem. Lett. 17 (2019) 1539–1551, https://doi.org/10.1007/s10311-019-00895-9.
[48] G.Z. Ramon, M.C.Y. Wong, E.M. V Hoek, Transport through composite membrane, part 1: is there an optimal support membrane? J. Membr. Sci. 415 (2012) 298–305, https://doi.org/10.1016/j.memsci.2012.05.013, 416.
[49] R. Pang, K. Zhang, Fabrication of hydrophobic fluorinated silica-polyamide thin film nanocomposite reverse osmosis membranes with dramatically improved salt rejection, J. Colloid Interface Sci. 510 (2018) 127–132, https://doi.org/10.1016/j.jcis.2017.09.062.
[50] B. Khorshidi, I. Biswas, T. Ghosh, T. Thundat, M. Sadrzadeh, Robust fabrication of thin film polyamide-TiO2 nanocomposite membranes with enhanced thermal stability and anti-biofouling propensity, Sci. Rep. 8 (2018) 784, https://doi.org/10.1038/s41598-017-18724-w.